Available online at www.sciencedirect.com
SCIENCE DIRECT®
ELSEVIER
Mechanical Systems and Signal Processing 20 (2006) 1696–1724
Mechanical Systems and Signal Processing
www.elsevier.com/locate/jnlabr/ymssp

Resonance tracking in a squeeze-film levitation device

Ran Gabay, Izhak Bucher*

Dynamics and Mechatronics Laboratory, Faculty of Mechanical Engineering, Technion Israel Institute of Technology, Haifa 32000, Israel

Received 1 November 2004; received in revised form 9 March 2005; accepted 13 March 2005
Available online 13 June 2005

Abstract

An adaptive method, with which an excitation frequency is continuously varied to obtain maximal oscillation levels, is developed. It is shown that this approach yields the best mechanical efficiency and it is thus essential when the available input power is restricted. The method is demonstrated on a specific apparatus, a squeeze-film levitation device, to obtain maximal levitation height of a floating object. The proposed method uses a minimal amount of frequency dither to revive an identification process that is otherwise singular. With this identified model, the algorithm seeks the best momentary excitation frequency. The algorithm is validated in a simulation and on dedicated experimental apparatus.

Keywords: Resonance tracking; Adaptive excitation; Squeeze-film levitation; Dither

1. Introduction

This paper deals with an adaptive excitation scheme trying to generate the largest possible amplitude of vibration under limited input power. The sought method requires the identification of relevant system parameters and the selection of the best excitation frequency to excite the system with. When the vibrating system tends to vary with time, a suitable identification process should be able to track these variations in order to maintain near-optimal performance in

*Corresponding author. Fax: +972 4 8324533.
E-mail address: bucher@technion.ac.il (I. Bucher).
URL: http://dynamics.technion.ac.il.

0888-3270/$ - see front matter © 2005 Elsevier Ltd. All rights reserved.
doi:10.1016/j.ymssp.2005.03.001

real-time. Non-linear behaviour poses an additional difficulty as such systems no longer have a fixed-parameter linear approximation for a range of applicable amplitudes [1]. In the focus of this paper is a squeeze-film levitation device (SFLD) (see [2] for a detailed description). The non-linear behaviour of a compressible fluid under normal vibration yields a load-carrying average pressure. This average pressure is proportional to the square of the surface vibration amplitude. Therefore, the levitation apparatus is designed to create relatively large amplitudes (several micrometres) at a specific ultrasonic frequency. In this device the excitation signal must not deviate from a narrow frequency band, where non-contacting levitation of an object occurs. The physical limitation of the applicable excitation frequency range restricts the amount of available information about the system. This may render the on-line identification task extremely difficult, often nearly singular. For non-linear systems, the commonly employed algorithms (e.g. phase-locked loop (PLL)) [3–5]. These algorithms assume a fixed phase-difference between the excitation and the response at a resonance, may fail. It has been shown that the phase difference (between the excitation and the response) in a SFLD, at resonance, depends on the operating conditions and cannot be used to tune a PLL to attain maximum response as in linear electrical systems (see [2, Fig. 7]). A failure in the identification process would make a squeeze-levitation device completely inoperable.

It is evident that the requirement to maintain an optimal mode of operation necessitates a real-time identification scheme which is (i) sufficiently simple to be implemented in real-time, and (ii) being robust against failure.

In a typical squeeze-film levitation system such as shown in Fig. 1, the best levitation is achieved when operating in frequencies at which the combined device (incorporating the electromechanical and fluid parts as shown in Fig. 1) is most compliant. One expects an optimal excitation frequency to reside in the vicinity of one of the resonance frequencies as illustrated in Fig. 2. In order to maintain the levitation, one is compelled to generate an excitation signal sufficiently close to a suitable frequency at which the structural compliance is maximal. Indeed, Fig. 2 illustrates that a small deviation from the resonance frequency can reduce the amplitude of vibration considerably to a level where no levitation can take place.

In this work, it was chosen to fit a black-box geometric model describing the response curve around a single resonance. This model can be viewed as a series expansion of the response around a specific frequency. Indeed in Fig. 3 an off-line measurement of the response curves was performed on the system appearing in Fig. 1 in the vicinity of a chosen natural frequency. This measurement illustrates that when the excitation frequency is sufficiently close to the natural frequency, the response curve can indeed be approximated reasonably well by a low-order polynomial.

The proposed algorithm contains a real-time identification scheme trying to reconstruct this changing frequency-dependent curve in real-time. Due to the fact that the response curve is steep (low damping) off resonance, the allowed excitation frequencies are limited to a narrow band. In order to increase the amount of available information to the curve-fitting part, the concept of dithering is introduced. Dithering allows to statistically reduce the algorithm's tracking error by enriching the identification scheme [6]. The enrichment of the available data is achieved by perturbing (dithering) the excitation frequency around the desired frequency.

As will be shown, the identification of the required model needs some additional excitation in the form of a dither signal without which, it may fail. Dither is most commonly used to reduce the effect of quantisation of under-sampled and re-sampled signals for audio and image-processing

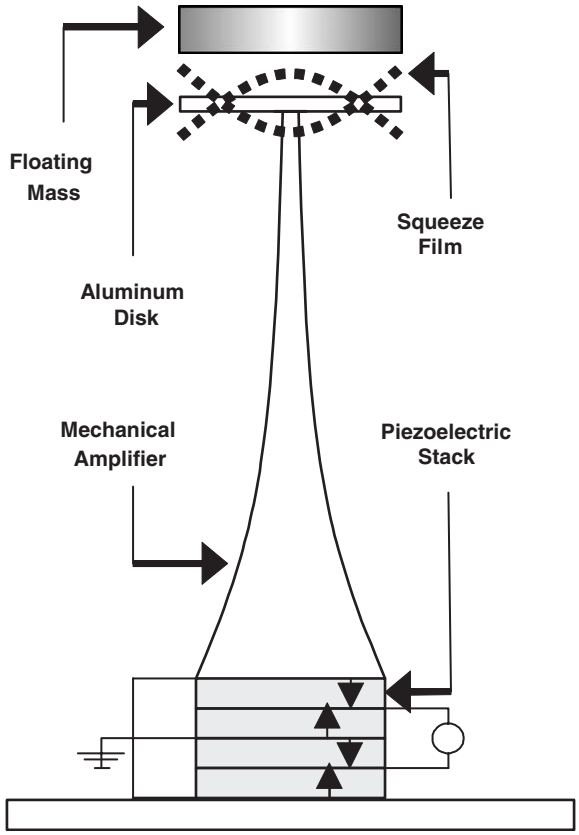

Fig. 1. Squeeze-film levitation device schematics.

applications [7]. Dither is also used to enhance the accuracy of a radome slope estimation [8] and to improve the missile autopilot performance [9]. None of the mentioned references provides any quantitative or theoretical analysis of the effect of dither on the identifiability of the model.

With this model at hand, it is possible to estimate the appropriate excitation frequency needed to maintain maximum operational amplitude, subject to electrical power limitations.

Salbu studied squeeze-film devices [10] and showed how high-frequency vibrations could be used to levitate a floating object. In this work some simplified analysis was provided, suggesting a physical explanation for the levitation phenomenon. Minikes and Bucher [2] have built such a levitation device incorporating a mechanical amplifier (Horn—see Fig. 1) and developed a numerical model coupling the mechanical and electrical parts to the fluid part. These works concluded with a statement saying that in order to operate SFLDs in an optimal manner, a resonance tracking algorithm should be used.

The most common resonance tracking algorithm in use is based on a PLL [11,12] that is in use in many electronic and electrical devices. For mechanical devices, Sun et al. [3] implemented a PLL-based scheme for MEMS devices where sufficient amplitude is required for good sensitivity. Tapson and Greene [4] also used PLL to keep an electro-mechanical device in an appropriate

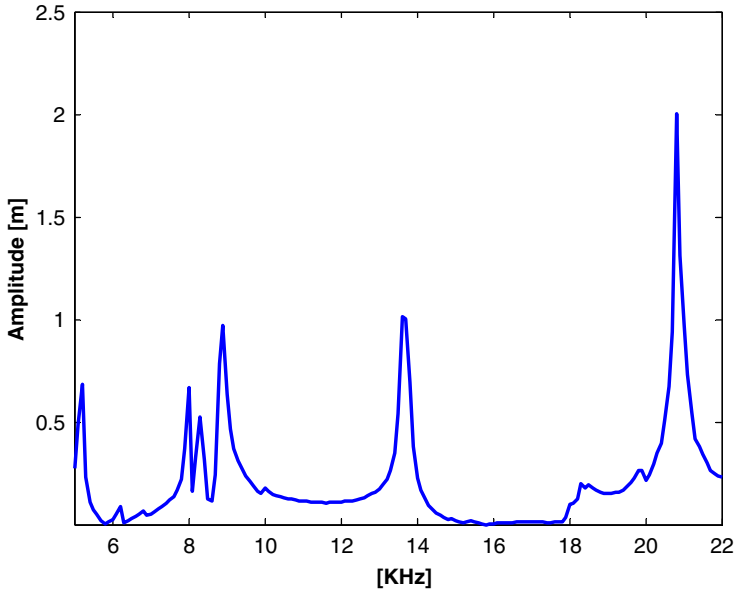

Fig. 2. Response amplitude of the flexible aluminium disk vs. frequency.

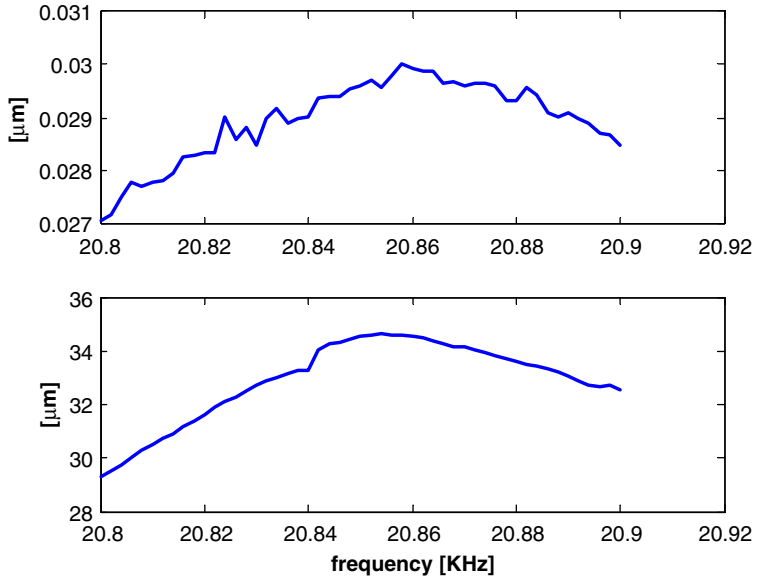

Fig. 3. Measured amplitude of vibration (top) and levitation height (bottom) vs. frequency.

operating mode, Tapson has also proposed a technique called admittance locking [5] which seems attractive, but was proven only for, well-behaved systems. PLL and admittance locking both rely on perfect linear behaviour of the systems that are to be driven by these algorithms. The presented method tries to overcome the deficiencies of the previously proposed methods at the expense of

slightly more sophisticated algorithm that necessitates a digital signal processor rather than analog circuitry.

Mendel et al. [13,14] deal with recursive estimation algorithms implementation and analysis that is a key component to the proposed algorithm. Recursive estimation algorithms are discussed extensively in the literature and considered well understood.

The paper is structured as following: Sections 2 and 3 describe the problem and the proposed resonance tracking approach detailing the identification and optimisation stages. In Section 3, a detailed analysis of the influence of dither is presented. In Section 4 the properties of the proposed method are studied via simulations and an experimental study. Section 5 concludes the paper with a summary of the main points that were addressed.

2. Statement of the problem

The proposed method can be viewed as an optimisation problem where an unknown time-varying system is sought to be driven at a large as possible amplitude of vibration. Although a rather generic algorithm is presented, a particular physical system, namely a SFLD [2] is being used to illustrate the physical and mathematical constraints. The SFLD seeks to maintain the largest possible levitation level by injecting the energy at a frequency where the electromechanical energy conversion is most effective.

2.1. Definition of the problem

The presented algorithm can be viewed as a variant of a resonance tracking algorithm, but here, unlike other studies, an unknown model of the entire system is dealt with. As will be shown later, the optimal operation of this device requires that the excitation frequency will be sufficiently close to the resonance frequency of the system. Let $\omega_0(t)$ denote the instantaneous optimal frequency and let $h(\omega, t)$ be the levitation height. The general problem can be formulated as

$$\omega_0(t) = \max_{\omega}\{h(\omega, t)\} \tag{1}$$

$$\text{subject to} \quad \omega_0 - \Delta \leqslant \omega \leqslant \omega_0 + \Delta. \tag{2}$$

Due to power efficiency considerations, it is expected that the bounds $\omega_0 \pm \Delta$ defining the region in which the system operates correctly will be quite narrow.

The levitation gap to be maximised is a function of the state vector, $x(t)$

$$h(\omega, t) = f(x(t)). \tag{3}$$

The state-vector obeys a non-linear differential equation that is controlled by a function of the excitation frequency and time $-q(x, \omega, t)$, but is also subject to slowly varying external disturbance vector $-d(t)$. The state-vector evolves according to unknown differential equations of the form:

$$\dot{x} = q(x, \omega, t) + d(t). \tag{4}$$

The largest difficulty in solving Eqs. (1)–(2) stems from the fact that the variables in Eq. (4) are unknown. In fact there is no prior knowledge about the exact functional dependence of h upon ω. Due to the severe restriction bounding the allowable frequency to within $\omega_0 \pm \Delta$, the amount of

information that can be collected about $h(\omega, t)$ is rather limited. Furthermore, upon convergence, the excitation frequency is nearly fixed and therefore the ability to accommodate changes in the system decreases considerably. This fact will be addressed in detail further on.

2.2. The relationship between excitation frequency and energy conversion efficiency

Consider a piezoelectric subsystem driving a mechanical vibrating system (see Fig. 1). It is shown here that the (locally) minimal amount of instantaneous power, for a given amount of mechanical work, is drawn from the driving power supply when the excitation frequency equals a natural frequency. The immediate implication of this fact is that an optimal driving mode, in the sense of energy and limited power utilisation, is achieved by a resonance tracking algorithm such as the one proposed here.

$u(t)$, the steady-state response to a sinusoidal excitation $g(t) = G\mathrm{e}^{i(\omega t-\beta)}$ (be it voltage or external force), can be expressed as

$$u(t) = U\mathrm{e}^{i(\omega t-\theta)}. \tag{5}$$

The equations of motion in a matrix form can be rewritten in the so-called H-form [15] of the combined piezoelectric and mechanical systems (in steady state):

$$(-\omega^2 M_{uu} + i\omega C_{uu} + H_{uu})U\mathrm{e}^{i(\omega t-\theta)} = G\mathrm{e}^{i(\omega t-\beta)}, \tag{6}$$

where U, G are the (real) response and force (voltage) amplitudes and θ, β are phase angles. Here M_{uu}, C_{uu}, H_{uu} are the mass, damping and stiffness matrices, respectively, where the stiffness matrix capture both the mechanical and piezoelectric contributions [15]. It is assumed, that the damping is light and can thus be considered proportional [16].

In order to find an expression for the efficiency, the definition of the mechanical power as [16, pp. 107], is considered

$$P(t) = P_R - iP_I = \dot{\bar{u}}^T(t)g(t), \tag{7}$$

where P_R, P_I are the active and reactive power terms, respectively.

The proof is deferred to Appendix A showing that in the vicinity of the lth natural frequency (ω_l), the total power $P = \sqrt{P_R^2 + P_I^2}$, as a function of the excitation frequency ω, of the system in Eq. (6) becomes

$$P = \frac{\left(\psi_l^T G\right)^2}{2\zeta_l\omega_l}\sqrt{1 + \left(\frac{\omega_l - \omega}{\zeta_l\omega_l}\right)^2}, \tag{8}$$

where ψ_l is the lth normal mode and ζ_l is the relevant modal damping ratio.

It is clear from Eq. (8) that the total power (for a fixed amount of input power, i.e. $\psi_l^T G = \text{const.}$) is minimised when $\omega_l = \omega$.

The maximal amount of power that can be delivered by a power source (e.g. high-voltage amplifier in the piezo-ceramic case) limits the amount of power (or displacement) that can be delivered to the controlled medium. Nearly no power is wasted in the form of circulating reactive power when the excitation frequency matches exactly one of the natural frequencies. The efficient

conversion of electrical to mechanical power maximises the level of levitation which is the goal in this case.

3. The proposed algorithm

The proposed algorithm consists of two major stages, a model estimation stage and an optimisation stage. The estimation stage is based on a recursive least squares (RLS) estimation algorithm [13] and the optimisation stage is based on the line search minimisation algorithm [17]. A block diagram of the algorithm is given in Fig. 4. The objective of the optimisation stage is to minimise some performance index, $J(\omega)$, which is related to the system's dynamics. This

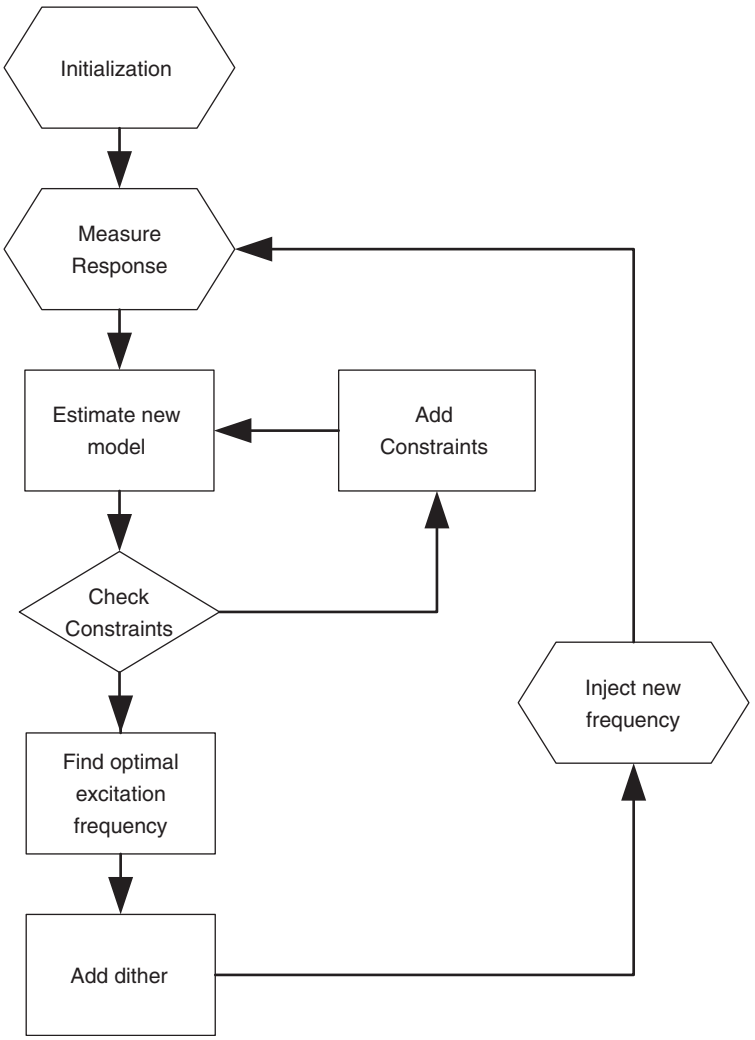

Fig. 4. Algorithm block diagram.

performance index is derived from the instantaneously estimated model. With the current performance index in hand, one can seek the excitation frequency under which the best performance can be achieved, and apply it to the system. The physical limitations and some safeguards add constraints to the search and while preventing the algorithm from diverging, they increase the difficulty in both the identification and optimisation stages. These difficulties are treated by analysing the physical, numerical and mathematical behaviour of every stage in the algorithm and implementing some modifications. It is shown that without the proposed modifications, the search for an optimal excitation frequency may fail completely.

3.1. The algorithm

Since the dynamical model of the system, as well as the external disturbance (Eq. (4)), are unknown, a parametric model of the instantaneous levitation height, $h(\omega)$ is chosen. This parametric model is directly related to the amplitude of vibration in the vicinity of the desired operation frequency. It is expected that the performance index, being directly related to the frequency response function, would have an optimum at the resonance frequency of the complete system. For sake of convenience, the optimisation stage is re-cast as a minimisation problem and therefore the performance index is defined as

$$J(\omega) \triangleq -h(\omega). \tag{9}$$

For the SFLD, maximum levitation height would yield a local minimum of $J(\omega)$.

3.1.1. Modelling for identification

Optimisation methods often use a first- or second-order approximation of the performance index, $J(\omega)$

$$J(\omega) \approx J(\omega_0) + \left.\frac{\partial J(\omega)}{\partial \omega}\right|_{\omega=\omega_0} (\omega-\omega_0) + \frac{1}{2}\left.\frac{\partial^2 J(\omega)}{\partial \omega^2}\right|_{\omega=\omega_0} (\omega-\omega_0)^2 + O(\omega^3). \tag{10}$$

The difficulty with the current problem is that the performance index is known at a rather narrow frequency range, therefore both $(\partial J(\omega)/\partial\omega)$ and $(\partial^2 J(\omega)/\partial\omega^2)$ cannot be accurately and robustly estimated.

Rather than estimating the first and second derivatives by differentiating the measured instantaneous values of $J(\omega)$, a smoothed estimate of these quantities is generated.

The chosen method ties $J(\omega_0), (\partial J(\omega)/\partial\omega)$ and $(\partial^2 J(\omega)/\partial\omega^2)$ in a model that resembles the Taylor series in Eq. (10), namely

$$J(\omega) = a_0 + a_1(\omega-\omega_0) + a_2(\omega-\omega_0)^2 + a_3(\omega-\omega_0)^3 + O((\omega-\omega_0)^4). \tag{11}$$

It is worth mentioning that a second-order model could be insufficient when the performance index has some asymmetric behaviour and when the measured range is not small. As an illustration (in Fig. 5) two models are fitted to a set of measurements. It is quite clear that the extreme point appears at a different location for the second- and third-order models.

The parametric model proposed in Eq. (11), when fitted to a set of measurements, provides a smoothed estimate to the measured response curve. On the other hand, numerical differentiation of the measured data (as a means to realise Eq. (10)), would amplify the measurement noise

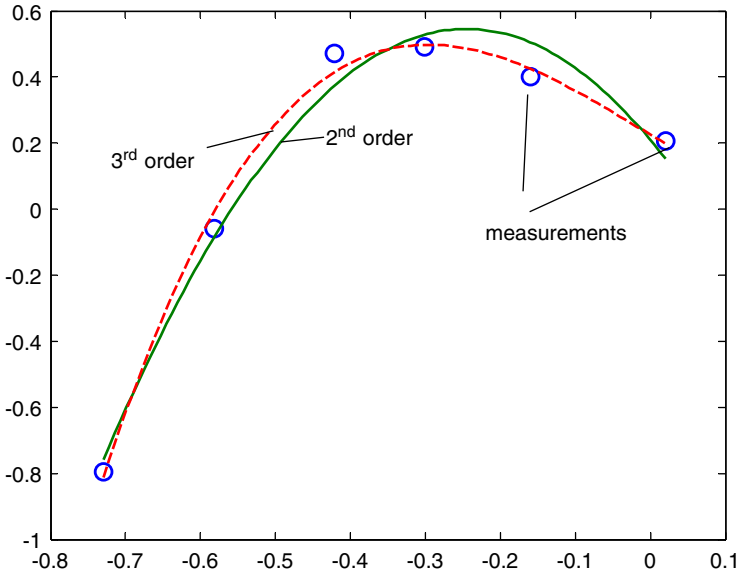

Fig. 5. Illustration of a second- and third-order approximation of the performance index model.

considerably. For this very reason, the proposed approach uses a parametric model (polynomial) that is fitted to the measured response prior to its differentiation. Once a model has been fitted, the differentiation can be performed analytically thus providing a smooth expression for the curvature.

In Fig. 3, the curves describing the amplitude of vibrations of the floating disk and levitation gap ($\bar{h}$) vs. the excitation frequency are presented. It can be seen that both curves achieve their maximum values nearly at the same frequency and therefore one can rely on any one of these curves as the performance index. Still, the floating disk vibrations are considerably smaller than the levitation gap and therefore the gap seems to provide a better signal-to-noise ratio. The curve is modelled as a third-order polynomial, which is equivalent to Eq. (10)

$$\bar{h}(\omega) \cong p_3\omega^3 + p_2\omega^2 + p_1\omega + p_0. \tag{12}$$

Due to the different scale of the frequency (kHz range) and the levitation gap (μm range) some numerical difficulties may arise when using such a polynomial. Therefore, the frequency domain is scaled to be of $O(1)$ by using the following transformation

$$\tilde{\omega} = \frac{\omega - \omega_0}{S}, \tag{13}$$

where ω_0, S are selected to attain appropriate mapping. The performance index was defined in Eq. (9), therefore the performance index parametric model is defined as

$$J(\omega) \triangleq -\bar{h}(\omega) \approx a_3\tilde{\omega}^3 + a_2\tilde{\omega}^2 + a_1\tilde{\omega} + a_0. \tag{14}$$

The performance index now has a minimum point where the levitation is at its maximum. By estimating a coefficient vector, $\underline{a} = [a_3 \ a_2 \ a_1 \ a_0]$, with the levitation height measurements, an approximation of the response curve is formed.

3.1.2. Calculating the optimal excitation frequency

Having identified the performance index the optimal excitation frequency consisting of the minimum point can be extracted. Since the system is very sensitive to changes and the estimated performance index has a finite accuracy, rapid frequency changes must be avoided. The calculation of the new excitation frequency is done by applying a line search optimisation [17] in two stages—the first stage determines the direction of the optimal frequency and in the second stage the step size is computed.

A third-order polynomial $J(\tilde{\omega})$ may materialise in one of two curve types: (i) a curve with an extreme point or (ii) a curve with no extreme point (see Fig. 6). For type (i)-curve the minimum point is

$$\omega_{\text{opt}} = \left(-2a_2 + 2\sqrt{a_2^2 - 3a_3a_1}\right)/6a_3. \tag{15}$$

Therefore, the optimal frequency step is $\Delta\omega = \omega_{\text{opt}} - \omega_k$. If the estimated performance index has no minimum point (a possible case for third-order polynomial) the optimal direction is determined using Newton's step [17]:

$$\Delta\omega = -\left(\upsilon + \frac{\mathrm{d}^2 J}{\mathrm{d}\omega^2}\right)^{-1} \frac{\mathrm{d}J}{\mathrm{d}\omega}, \tag{16}$$

where υ is the Levenberg–Marquet addition [17] to avoid singularity.

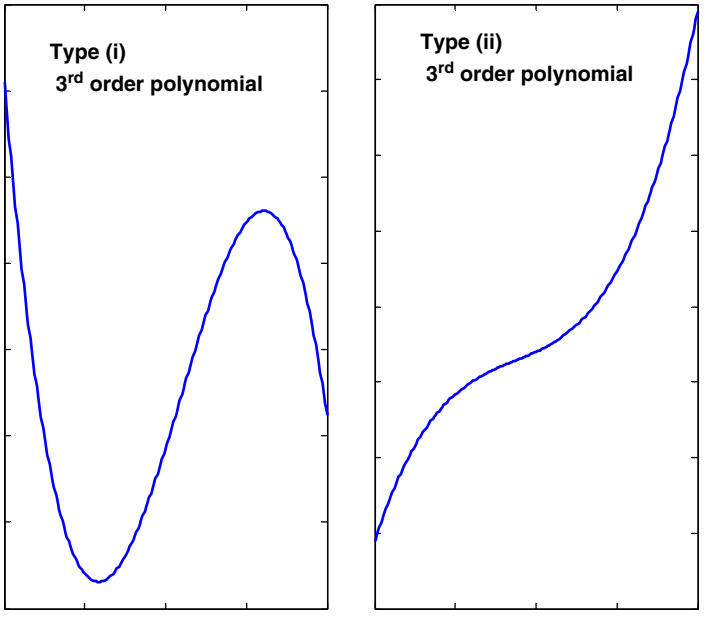

Fig. 6. Possible types of third-order polynomials estimation of the performance index.

In order to determine the step-size of the excitation frequency, two constraints are applied. The first constraint is meant to prevent too big steps

$$\omega_k - B < \omega_{k+1} < \omega_k + B, \tag{17}$$

where B is an application specific parameter. The second constraint prevents too drastic changes with respect to the identified performance index. This constraint is implemented using Armijo's rule [17], which adds damping to the line search and prevents large changes. The Armijo rule is defined as

$$\omega_{k+1} = \omega_k + \lambda\Delta\omega, \tag{18}$$

where the parameter $\lambda, (\lambda \leqslant 1)$ determines the actual step size. This parameter is calculated from [17]

$$\hat{J}(\omega_k + \lambda\Delta\omega) - \hat{J}(\omega_k) < \lambda \left(\left. \frac{\mathrm{d}\hat{J}}{\mathrm{d}\omega} \right|_{\omega=\omega_k} \right) \Delta\omega. \tag{19}$$

The new calculated frequency is injected to the system becoming the new excitation frequency.

3.1.3. Estimating the performance index

There is a variety of estimation algorithms able to extract a time-varying linear model in real time from measured data. Some of the more acceptable methods are the least mean squares (LMS) [18], recursive least squares (RLS) and the extended kalman filter (EKF) [13]. The chosen estimator here is the RLS estimator which is fast and accurate enough for the purpose while being sufficiently simple for a real time implementation. Moreover, RLS does not require any assumptions regarding the dynamics of the model (as EKF does). RLS is based on the well-known least squares (LS) method [13] that provides a smoothing effect.

In order to adapt the RLS to our system some definitions are in order. The parameter vector to be estimated (the performance index coefficients Eq. (14)), is

$$\underline{a} \triangleq [a_3 \;\; a_2 \;\; a_1 \;\; a_0]^T. \tag{20}$$

It is assumed that each measurement conforms to the model

$$z_k = J(\tilde{\omega}_k) + v_k, \tag{21}$$

where v_k is an added measurement noise. The observation matrix, H, can now be defined

$$\underline{h}_k = [\tilde{\omega}_k^3 \;\; \tilde{\omega}_k^2 \;\; \tilde{\omega}_k \;\; 1]^T \Rightarrow H = \begin{bmatrix} h_1^T \\ \vdots \\ h_N^T \end{bmatrix}. \tag{22}$$

Here k—iteration time index and $\tilde{\omega}_k$—the scaled frequency at time k.

The linear model in Eq. (21) can be rewritten for the kth iteration as

$$\hat{z}_k = h_k^T a_k + v_k. \tag{23}$$

The RLS estimator is advanced (in covariance form) [13], by

$$\hat{a}_{k+1} = a_k + K_{k+1}(z_{k+1} - h_{k+1}^T a_k), \tag{24}$$

where the gain K_{k+1} is given as

$$K_{k+1} = P_k h_{k+1}(h_{k+1}^T P h_{k+1} + w_{k+1}^{-1})^{-1} \tag{25}$$

and P_k is the covariance matrix, which is recursively computed by

$$P_{k+1} = (I - K_k h_k^T)P_k. \tag{26}$$

Note that w_k is a weight that adds a fading memory effect to the algorithm. A common use of the fading memory is to define a constant forgetting factor γ ($\gamma \leqslant 1$) and use [13]:

$$w_k = \gamma^{-1}. \tag{27}$$

For a later analysis the recursive dependence of the information matrix, P^{-1}, on the excitation frequency via is shown

$$P_{k+1}^{-1} = P_k^{-1} + h_{k+1} w_{k+1} h_{k+1}^T. \tag{28}$$

Using Eqs. (24)–(26), a real-time estimation of the performance index model (Eq. (14)) is obtained and the optimal excitation frequency can be extracted as described in Section 3.1.2.

3.1.4. Initialisation of the algorithm

The standard method of initialising a recursive estimator, such as RLS, is using zero initial value for the estimation object [13]

$$\underline{a}_0 = \underline{0} \tag{29}$$

and the initial covariance matrix is defined as a diagonal matrix

$$P_0 = \beta I, \tag{30}$$

where β is some large value. A boot-strapping procedure is employed where the levitation height is being measured in a small range of frequencies. These measurements can be used to compute an initial vector of parameters $\underline{a}_0$, the initial frequency $\tilde{\omega}_0$ and the initial covariance matrix P_0 via a batch LSs [13].

In order to assure that all parameters in $\underline{\hat{a}}_k$ have an equal sensitivity for changes in all directions in the parameter space, a transformation T_n that yields a close to unity scaling, has to maintain

$$a_0 = T_n[1 \;\; 1 \;\; 1 \;\; 1]^T. \tag{31}$$

This leads to the definition of the transformation—$T_n = \mathrm{diag}(\underline{a}_0)$.

Now the observation matrix (Eq. (22)) becomes

$$H_k \triangleq \left[\tilde{\omega}_k^3 \;\; \tilde{\omega}_k^2 \;\; \tilde{\omega}_k \;\; 1\right] T_n \tag{32}$$

and the newly obtained covariance matrix, becomes

$$P_0^{(\mathrm{scaled})} = T_n^{-1} P_0 (T_n^T) - 1. \tag{33}$$

In this section the basic structure of the proposed algorithm was introduced. Although the algorithm is composed of known and well-proven methods for the sub-tasks, some difficulties

arise when the sub-tasks are combined to form a single algorithm. These difficulties are discussed in the following section and some improvements are introduced to overcome them.

3.2. Algorithm difficulties and improvements

In the previous section the basic algorithm was introduced. As was expected, convergence to an optimal excitation frequency in stationary cases is achieved, as can be seen in Fig. 7. When testing the algorithm for non-stationary cases (see Fig. 8), it fails to track changes in the model. Indeed Fig. 8 illustrates this failure which is caused by the confinement of the excitation frequency to a relatively small region. Once the system achieves steady state, the excitation frequency remains nearly fixed and no new information is added to the identification algorithm. This renders the identification equations singular, leading to the wrong excitation frequency. In this section, several modifications to the identification algorithm, that are crucial to its successful operation, are described and analysed.

3.2.1. Analysing the effect of insufficient information

The influence of the restriction to a narrow frequency region can be analysed mathematically. In the observation matrix, H, which is defined in Eq. (22), it can be observed that once no new information is being added, it has identical columns and may thus loose rank. Indeed, examining the off-line representation of the identification problem (see [13]):

$$\underline{\hat{a}} = (H^T H)^{-1} H^T z \tag{34}$$

it can be observed that the matrix $H^T H$ may become ill conditioned and cannot be inverted to provide a meaningful estimate of the sought polynomial. When the observation matrix H looses

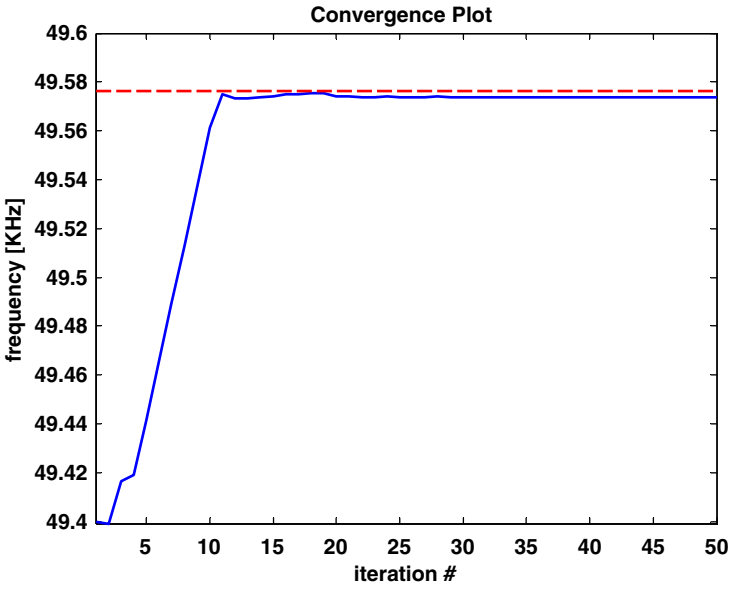

Fig. 7. Convergence of the algorithm.

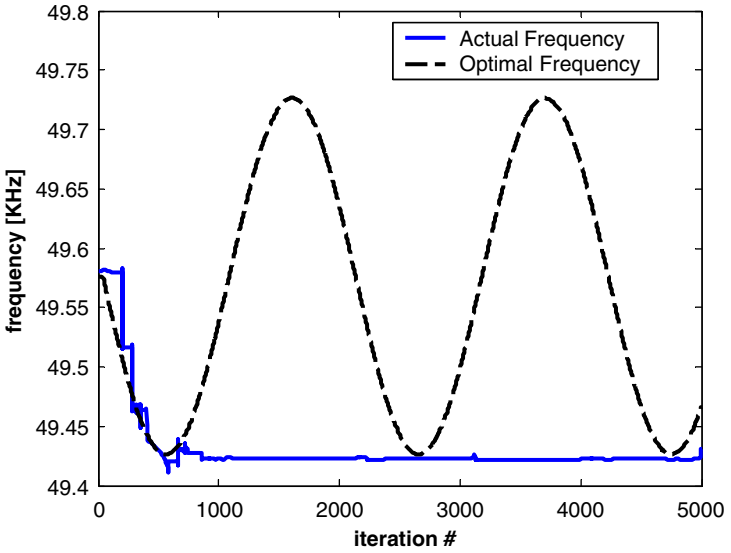

Fig. 8. The basic algorithm's failure in tracking frequency changes.

its full rank, the identification system looses its identifiablity property [14]. A similar conclusion can be obtained from the recursive definition of the information matrix (Eq. (28)), it can be seen that the rank-one matrix $(h_k w_k h_k^T)$ is being added to the previous information matrix in each iteration. For constant frequency $\tilde{\omega}_k$, the same rank 1 matrix (up to a scalar) is added and therefore no new information is added. In other words, in this case information is added in a single direction in the parameters space so eventually the information matrix looses its rank. Two properties of the estimator are affected from this behaviour—the estimator's information (covariance) and the accumulated memory.

The information matrix P^{-1}, defined as [13]

$$P^{-1} \triangleq H^T H. \tag{35}$$

It becomes singular due to the lack of information (when $H^T H$ looses its rank) and equivalently the covariance matrix—P_k shows larger variance of the parameters.

The algorithm was enhanced using several techniques to overcome the lack of information and memory saturation as described below.

3.2.1.1. Adding dither. In order to assist the algorithm to gain more from the measured information, a small frequency dither, δ, is added. The dither is a small random addition to the excitation frequency causing slight fluctuations around the optimal frequency, increasing the amount of measurement points. The added dither should be sufficiently large to achieve the desired statistical performance; on the other hand, the dither should be sufficiently small to keep the excitation frequency within the allowed bounds. The analysis presented below, relates the dither level to the improvement in the identification process.

3.2.1.2. Dither analysis. As statistically defined errors are dealt with here, the estimation error boundaries as a function of the dither level need to be found. Assuming that the random measurement noise has a Gaussian distribution with zero mean, i.e.

$$v \sim \mathcal{N}(0, \sigma_v^2). \tag{36}$$

And the dither is also sampled from Gaussian distribution

$$\delta \sim \mathcal{N}(0, \sigma_\delta^2). \tag{37}$$

For this analysis, the optimal excitation frequency is assumed to be a constant—ω_0 and the actual excitation frequency becomes

$$\omega_k = \omega_0 + \delta_k. \tag{38}$$

The lower bound is calculated from the Cramer–Rao lower bound [13,14] that uses the Fisher information matrix, $M(\underline{a})$, [13,14] to calculate the covariance, $\bar{P}$, of the most efficient estimator:

$$\bar{P} \triangleq M(\underline{a})^{-1}. \tag{39}$$

The lower bound is achieved by the best unbiased estimator. Therefore, the covariance of the estimated vector $\underline{a}$ obeys

$$\mathrm{cov}(\underline{a}) \geqslant \bar{P}. \tag{40}$$

The effect of dither can be assessed via the Fisher information matrix since the addition of dither affects the amount of information obtainable from the measurements.

The analysis is focused on two types of errors

(i) The deviation of the estimation from the exact solution

$$\eta = \| \underline{a} - \underline{a}_{\mathrm{exact}} \|, \tag{41}$$

where it is proved later on that η is bounded from below by

$$\eta \geqslant \frac{\sigma_v}{\sqrt{6N\sigma_\delta^3}} \sqrt{(1 + 18\sigma_\delta^2 + 9\omega_0^2 - 6\omega_0^2\sigma_\delta^2 + 9\omega_0^4 + 9\sigma_\delta^6 + 9\omega_0^2\sigma_\delta^4 + 3\omega_0^4\sigma_\delta^2 + \omega_0^6)}, \tag{42}$$

here N is the number of measurements.

(ii) The second type of error is the variance of the performance index's gradient, e_g. The gradient determines the direction in which the frequency is changed; hence it is important for the line search stage. It is shown that this error has a lower bound, which is

$$e_g \geqslant \frac{5}{2N} \left(\frac{\sigma_v}{\sigma_\delta} \right)^2. \tag{43}$$

Proof. With the linear model defined in Eq. (23) and the above-mentioned assumptions, the Fisher information matrix can be expressed as [14]

$$M(\underline{a}) \triangleq \frac{1}{\sigma_v^2} E\{H^T H\}. \tag{44}$$

Substituting the excitation frequency from Eq. (38) into the observation matrix's definition (Eq. (22)), the observation matrix can be expressed as

$$H = \begin{bmatrix} (\omega_0+\delta_1)^3 & (\omega_0+\delta_1)^2 & (\omega_0+\delta_1) & 1 \\ \vdots & \vdots & \vdots & \vdots \\ (\omega_0+\delta_N)^3 & (\omega_0+\delta_N)^2 & (\omega_0+\delta_N) & 1 \end{bmatrix}. \tag{45}$$

It is easy to verify that without the dither this matrix has rank 1 as mentioned earlier. The matrix $H^T H$ which affects the solution process is (see Eq. (34))

$$H^T H = \begin{bmatrix} \sum_{i=1}^{N}(\omega_0+\delta_i)^6 & \sum_{i=1}^{N}(\omega_0+\delta_i)^5 & \sum_{i=1}^{N}(\omega_0+\delta_i)^4 & \sum_{i=1}^{N}(\omega_0+\delta_i)^3 \\ \sum_{i=1}^{N}(\omega_0+\delta_i)^5 & \sum_{i=1}^{N}(\omega_0+\delta_i)^4 & \sum_{i=1}^{N}(\omega_0+\delta_i)^3 & \sum_{i=1}^{N}(\omega_0+\delta_i)^2 \\ \sum_{i=1}^{N}(\omega_0+\delta_i)^4 & \sum_{i=1}^{N}(\omega_0+\delta_i)^3 & \sum_{i=1}^{N}(\omega_0+\delta_i)^2 & \sum_{i=1}^{N}(\omega_0+\delta_i) \\ \sum_{i=1}^{N}(\omega+\delta_i)^3 & \sum_{i=1}^{N}(\omega+\delta_i)^2 & \sum_{i=1}^{N}(\omega+\delta_i) & N \end{bmatrix} \tag{46}$$

and it also has rank 1 when no dither is present. For sake of simplicity, the dither is redefined as a relative amount of the frequency ω_0, i.e.

$$\delta \triangleq \alpha\omega_0, \tag{47}$$

where

$$\alpha \sim \mathcal{N}(0, \sigma_\alpha^2). \tag{48}$$

Substituting Eq. (47), in Eq. (46) and taking the expectation can apply the Cramer–Rao lower bound (Eq. (39)), to obtain

$$\bar{P} = \frac{\sigma_v^2}{6N\sigma_\alpha^6} \times \begin{bmatrix} \frac{1}{\omega_0^6} & -\frac{3}{\omega_0^5} & -3\frac{\sigma_\alpha^2-1}{\omega_0^4} & \frac{3\sigma_\alpha^2-1}{\omega_0^3} \\ -3\frac{1}{\omega_0^5} & 3\frac{\sigma_\alpha^2+3}{\omega_0^4} & 3\frac{\sigma_\alpha^2-3}{\omega_0^3} & -3\frac{\sigma_\alpha^4+2\sigma_\alpha^2-1}{\omega_0^2} \\ -3\frac{\sigma_\alpha^2-1}{\omega_0^4} & 3\frac{\sigma_\alpha^2-3}{\omega_0^3} & 3\frac{5\sigma_\alpha^4-2\sigma_\alpha^2+3}{\omega_0^2} & -3\frac{3\sigma_\alpha^4-2\sigma_\alpha^2+1}{\omega_0} \\ \frac{3\sigma_\alpha^2-1}{\omega_0^3} & -3\frac{\sigma_\alpha^4+2\sigma_\alpha^2-1}{\omega_0^2} & -3\frac{3\sigma_\alpha^4-2\sigma_\alpha^2+1}{\omega_0} & 9\sigma_\alpha^6+9\sigma_\alpha^4-3\sigma_\alpha^2+1 \end{bmatrix}. \tag{49}$$

The estimation error η can be calculated from a covariance matrix (P) via

$$\eta = \text{trace}(P). \tag{50}$$

Applying Eq. (50) to Eq. (49) leading to the result given at Eq. (42).

The gradient of the performance index $J(\tilde{\omega})$ (defined in Eq. (14)) can be calculated from

$$\frac{\mathrm{d}J}{\mathrm{d}\tilde{\omega}} = 3a_3\tilde{\omega}^2 + 2a_2\tilde{\omega} + a_1 \triangleq f^T \underline{a}, \tag{51}$$

where $f \triangleq [3\tilde{\omega}^2 \;\; 2\tilde{\omega} \;\; 1 \;\; 0]^T$ and $\underline{a}$ is defined in Eq. (20). The gradient's variance is obtained by computing

$$e_g \triangleq f^T P f. \tag{52}$$

Substituting Eq. (51) in Eq. (52) yields the gradient's variance lower bound as given in Eq. (43).

Investigating the effect of dither using norm inequalities: Define ε as the deviation from the exact noise-free solution of the estimation problem (Section 3.1.3), denoted as $\underline{a}_e$ (i.e. $\underline{a} = \underline{a}_e + \varepsilon$). The upper bound for $\|\varepsilon\|_2$ is obtained by employing matrix perturbation theory [20,21], to give (as proved below)

$$\|\varepsilon\|_2 \leqslant \frac{\sqrt{N}\sigma_v}{\sigma_{\min}(H)}, \tag{53}$$

where $\sigma_{\min}(H)$ is the smallest singular value of H (including the dither).

Proof. The observation matrix, H, can be written as a sum of a base matrix and a matrix of perturbations caused by the dither

$$H = H^0 + E, \tag{54}$$

where

$$H^0 = \begin{bmatrix} \omega_0^3 & \omega_0^2 & \omega_0 & 1 \\ \vdots & \vdots & \vdots & \vdots \\ \omega_0^3 & \omega_0^2 & \omega_0 & 1 \end{bmatrix}, \tag{55}$$

$$E = \begin{bmatrix} 3\omega_0^2\delta_1 + 3\omega_0\delta_1^2 + \delta_1^3 & 2\omega_0\delta_1 + \delta_1^2 & \delta_1 & 0 \\ \vdots & \vdots & \vdots & \vdots \\ 3\omega_0^2\delta_N + 3\omega_0\delta_N^2 + \delta_N^3 & 2\omega_0\delta_N + \delta_N^2 & \delta_N & 0 \end{bmatrix}.$$

Assume $\underline{a}_e$ is the exact solution of the system, Eq. (23) without measurement noise, becomes

$$(H^0 + E)\underline{a}_e = z, \tag{56}$$

when measurement noise (v) is present, the estimation error (ε) is added to yield

$$(H^0 + E)(\underline{a}_e + \varepsilon) = z + v. \tag{57}$$

Subtracting Eq. (57) from Eq. (56) have

$$(H^0 + E)\varepsilon = v. \tag{58}$$

The LS solution of Eq. (58) is formed using the generalised inverse [13]

$$\varepsilon = (H^0 + E)^+ v. \tag{59}$$

Looking at the norm of the estimation error and using the triangular inequality, it can be shown that

$$\|\varepsilon\| = \|(H^0 + E)^+ v\| \leqslant \|(H^0 + E)^+\| \|v\|. \tag{60}$$

In addition it can be shown that (see [20,21]),

$$\|(H^0 + E)^+\|_2 = 1/\sigma_{\min}(H^0 + E), \tag{61}$$

where $\sigma_{\min}(H^0 + E)$ is the minimal singular value of $(H^0 + E)$. Using Eq. (61) and Eq. (59) and making use of the fact that the measurement noise norm is

$$\|v\| = \sqrt{N\sigma_v} \tag{62}$$

the upper bound in Eq. (53) is obtained.

3.2.1.3. Effect of dither—discussion. Inspection of the dither bounds developed previously, adds some insight on the dither effect. The lower bounds reflect the fact that increasing the dither or the number of measurements, reduces (statistically) the error (see Eqs. (42), (43)). It was made clear that the measurement noise did not contribute to the enriching of the estimation process. Despite being a perturbation from the optimal value, the added dither does improve the conditioning of the identification process. The estimation error's lower bound (given in Eq. (42)) emphasises the fact that without dither the error grows to infinity. In addition, the estimation error depends on the frequency, ω_0, and on the dither level, σ_δ, as a third-order polynomial (in accordance with the performance index model). Moreover, the dependence of this error on the frequency emphasises the importance of the frequency normalisation that was described in Section 3.1.1 and in Eq. (13). Indeed, the estimation error decreases when the frequency, ω_0, approaches zero. This error is also affected by the dither level, but in the opposite way, the bigger the dither level the smaller the error becomes, as shown in Fig. 9.

It is important to examine the extreme values Eq. (42) can take. When $\sigma_\delta \ll 1$, Eq. (42) becomes

$$\bar{\eta} = \frac{\sigma_v}{\sqrt{6N}\sigma_\delta^3}\sqrt{1 + 9\omega_0^2 + 9\omega_0^4 + \omega_0^6}. \tag{63}$$

This expression reflects the fact that for a very small dither level, the sensitivity of the estimation error to the dither is very high. On the other hand, when $\sigma_\delta \to \infty$, Eq. (42) approaches asymptotically to

$$\lim_{\sigma_\delta \to \infty} \bar{\eta} = \frac{\sigma_v\sqrt{9\sigma_\delta^6}}{\sqrt{6N}\sigma_\delta^3} = \sqrt{\frac{3}{2}}\frac{\sigma_v}{\sqrt{N}}. \tag{64}$$

Eq. (64) reflects the fact that for a very large dither, the error does not depend on the dither level anymore and in fact it exhibits a standard behaviour of a LS estimator in respect to the noise level and number of measurements.

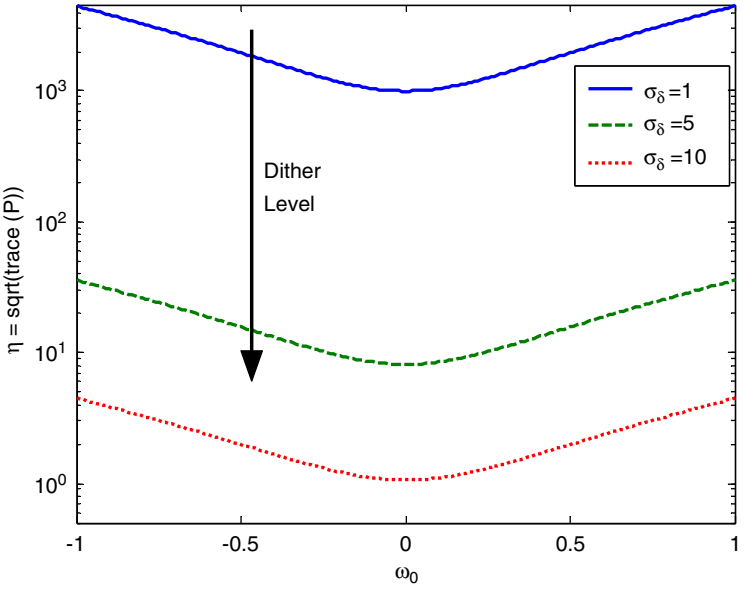

Fig. 9. The estimation error $\bar{\eta}$ as a function of ω_0 for various dither levels.

Inspecting the gradient error's lower bound (Eq. (43)), the term σ_δ/σ_v can be viewed as a signal-to-noise (S/N) ratio where the dither is playing the signal role. Simulations verify that the bounds that were developed are indeed lower bounds as can be seen in Fig. 10. Although the lower bound is not reached, the estimator tends toward it and the efficiency property of the LS estimator guarantees it is reached when $N \to \infty$. Plotting the analytical error-bound together with the actual deviation shows that the upper bound is very conservative, as can be seen in Fig. 11. Still, it does not violate the inequality in Eq. (53) proving its mathematical correctness.

3.2.2. *Saturation of the algorithm*

Since the standard fading memory approach (the w_k in Eq. (25)) fails to achieve its goal when insufficient information is obtained, the estimation process needs to be revived periodically. In this work, have used the covariance resetting technique [19,22] that resets the covariance matrix at fixed times to a pre-determined value:

$$P_k = \beta P_0. \tag{65}$$

This reset forces the estimator to apply an equal weight in all directions by disregarding past data. The resetting technique is applied in addition to the usual forgetting factor giving less weight to older data, but does not reset the sensitivity in the parameter space.

3.3. *Physical limitations*

The algorithm is based on the assumption that the performance index is a concave function. In some cases, usually following a rapid change in the system, the algorithm may erroneously estimate a convex function—a solution that is not in the allowed parameter space. When this

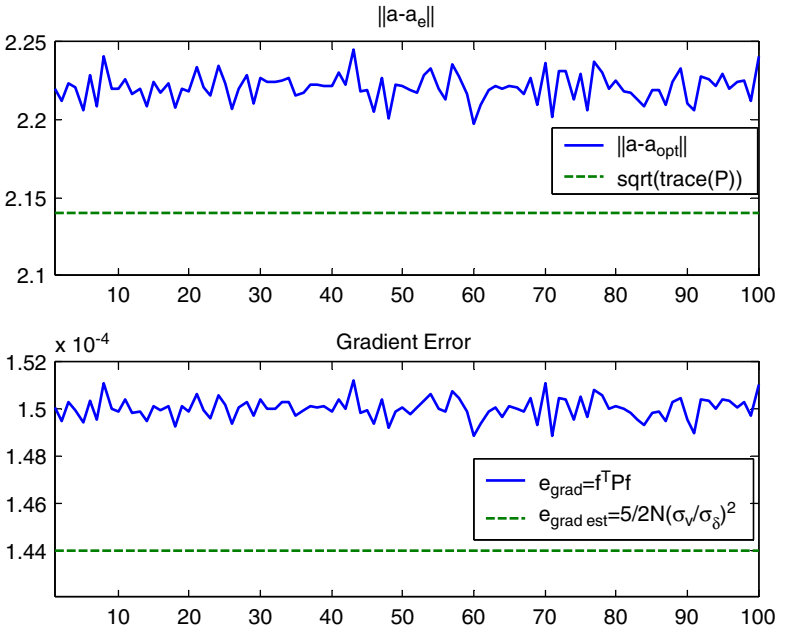

Fig. 10. Comparing between the actual estimation error and its lower bound, (top) performance index estimation error (bottom) gradient error variance.

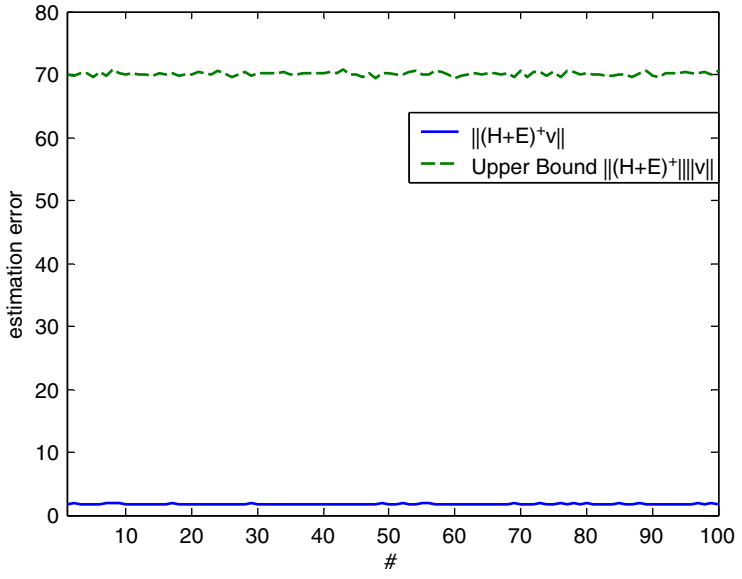

Fig. 11. Comparing the actual upper bound (simulated) and the analytically approximated upper bound of the estimation error.

happens, the algorithm seeks in the wrong direction in the parameter space and may thus perform inadequately. To prevent the algorithm form drifting in the wrong direction, a concavity constraint is enforced to the estimator. The concavity constraint can be expressed mathematically as: $\partial^2 J/\partial\tilde{\omega}^2 > 0$ and for the third-order polynomial model (Eq. (14)) it becomes

$$2a_2 + 6a_3\tilde{\omega} > 0. \tag{66}$$

Adding an inequality constraint to the estimator is a complex computational process [23], and for real-time computations it may be unacceptable. In order to simplify the application of this constraint it is transformed into an equality constraint:

$$2a_2 + 6a_3\tilde{\omega} = R, \tag{67}$$

where R ($R>0$) is the desired concavity. Eq. (67) can be added to the estimator as a dummy measurement that forces it to consider this constraint every time the estimated concavity is below a certain threshold.

4. Verification of the algorithm

In order to test the algorithm and to verify its ability to track the optimal excitation frequency, a series of tests were conducted. The algorithm was tested in a generic manner using series of computer simulations and a laboratory tests. The experimental squeeze-film levitation system is depicted in Fig. 1.

4.1. Simulation

In order to simulate the algorithm, a performance index was devised from a realistic simulation of the squeeze-film. The RLS was employed with a forgetting factor of $\gamma = 0.95$ (see Eq. (27)) and as can be seen in Fig. 7, the algorithm has kept its stability after converging to a fixed 'optimal' frequency.

In order to simulate slow variations in the optimal frequency, the performance index was shifted periodically around its minimum point. When testing the algorithm ability to track the optimal frequency, it seemed to have failed. Fig. 8 illustrates a typical behaviour of the basic algorithm where after a reasonable start seems to eventually lock on some fixed frequency, loosing its ability to track the changes. The failure to track the variations is attributed to the memory saturation and to the lack of information.

To overcome the problems associated with tracking and lack of information, two modifications have been suggested (as described in Section 3.2.2)—the covariance resetting technique and the addition of dither. In Fig. 12 the result of the simulation with the enhanced algorithm are shown, where the covariance is being reset every 50 iterations and dither $\sim\mathcal{N}(0, 5^2)$ was added. The algorithm now seems to track the changes with an improved accuracy, avoiding the memory saturation problem (as can be seen in Fig. 12). The achieved tracking error appeared to be normally distributed [24] with a mean bias of 0.37 Hz (0.0007%) and a standard deviation of 7.2 Hz (0.01%). These errors should be considered while keeping in mind that the bandwidth of the system (the frequency range between the -3 db points) is about 0.5% of the excitation frequency.

Through these simulations, the importance of the enhancements to the algorithm is demonstrated. It can be seen that by adding very little dither (0.01%) to the input frequency, the improvement in the performance is considerable.

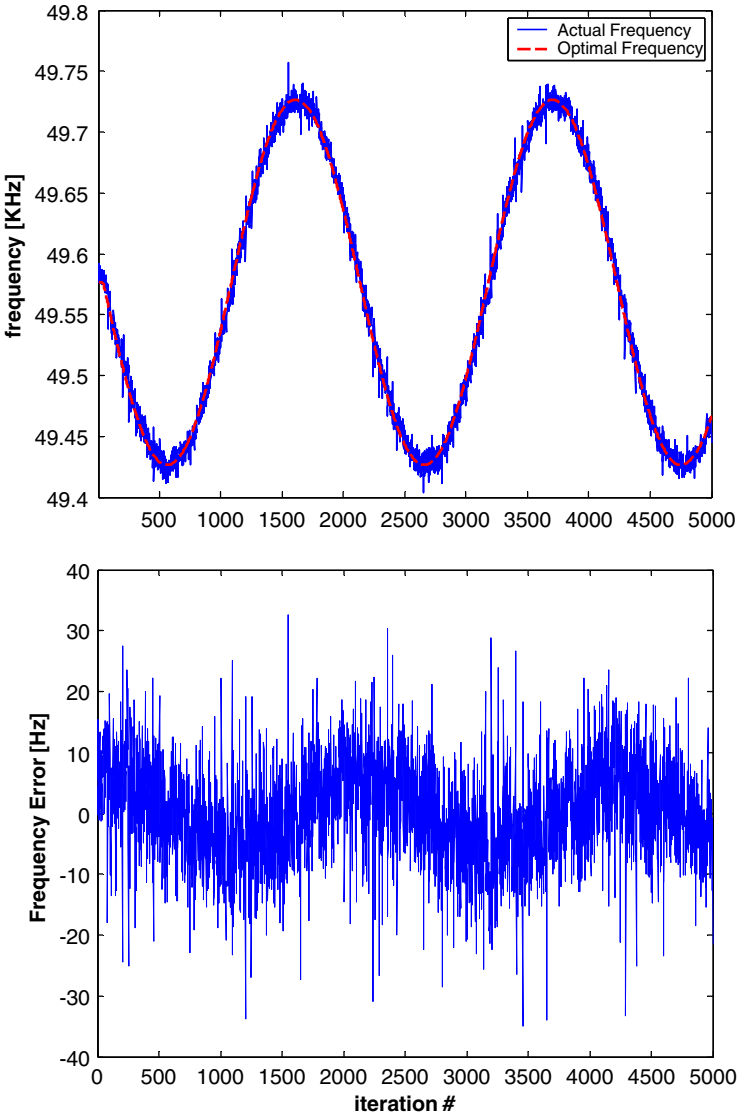

Fig. 12. Algorithm with dither and covariance resetting. Top: Tracking a time-varying optimal frequency. Bottom: The tracking error.

4.2. Experimental verification

In order to verify the algorithm's capabilities, an experimental system was built. This section describes in detail the physical system used for this verification and some results from this experiment are given.

4.2.1. The physical system—squeeze-film levitation system

The experimental system being used in this work can be distinguished by three main components: the electro-mechanical actuator, a thin air film and the levitated disk. As illustrated

in Fig. 1, the electro-mechanical actuator consists of a stack of piezoelectric disks (PZT-5A) connected to a mechanical amplifier (steel exponential horn) and a thin aluminium disk which serves as the driving surface and is connected to the tip of the horn. Relative normal oscillating motion between two surfaces, with the presence of a compressible fluid (such as air) in between, may generate a film (referred as a squeeze film) with a time average pressure higher than the surrounding pressure. The squeeze film effect occurs, for standard air, when the oscillations are at high frequencies (in the kilo-hertz range or more) with micrometre (or even submicrometre) vibration amplitudes. Under these conditions, equilibrium is established through a balance between viscous flow forces and compressibility forces. For detailed physical and mathematical description of this system see Minikes and Bucher [2]. The squeeze film effect develops a levitation force containing a constant component (the time average pressure) and a fluctuating part (at the frequency of excitation) where both attain a maximum simultaneously (see Fig. 3). This non-linear behaviour can be exploited to relate the average part in response (measured air-gap) and the harmonic input voltage amplitude and frequency. A similar comparison can be made with the system's output at the frequency of excitation (Fig. 3). Indeed, simulations and experiments show that at resonance, where the amplitude of vibration reaches its peak value, the mean gap attains a peak as well (see Fig. 3). This fact allows us to use either the average gap or the disc vibration as a measure for obtaining the highest levitation level as a function of the driving frequency. Some difficulties are encountered when one tries to predict the resonance frequencies of the overall system. The complex non-linear behaviour of the squeeze film and variations in the thermo-dynamical properties of the fluid create effects that cannot be predicted in linear system terms. Presuming that the system will resonate at the actuator's natural frequency (as shown at Fig. 2), could lead to severe inaccuracies as the levitated disk together with the squeeze film act as an added mass and therefore shifting the resonances frequencies. In their work, Minikes and Bucher [2] have revealed that the dynamical behaviour of the coupled squeeze film strongly depends on the mechanical structure and has an alternating behaviour at different frequency regions.

4.2.2. *Experiment*

The experimental system can be seen in Fig. 13 and it was designed according to the description in Section 4.2.1. Three optical sensors were added to serve as position indicators, measuring the levitation height of the floating mass. Using this system, the algorithm was verified under realistic conditions.

The experiment was carried out at a frequency close to an initially estimated resonance frequency and was conducted under the following conditions: dither level of $\sigma_\delta = 5\,\text{Hz}$, covariance resetting every 50 iterations, the external voltage amplitude to the piezoelectric stack was 140 V (nominally).

During normal operation (see Fig. 14) the system seems to work as expected with steady level of levitation of about 21 μm with an excitation frequency of about 21.05 kHz. The frequency fluctuations are around 20 Hz mostly due to the dither and covariance resetting.

In order to test the algorithm's performance under a rapid change in the system, a step change in the external voltage amplitude was applied changing the amplitude from 120 to 180 V after 350 iterations. Under this change, the resonance frequency is expected to change as both the piezoelectric stack and the air-film are somewhat non-linear with respect to the amplitude.

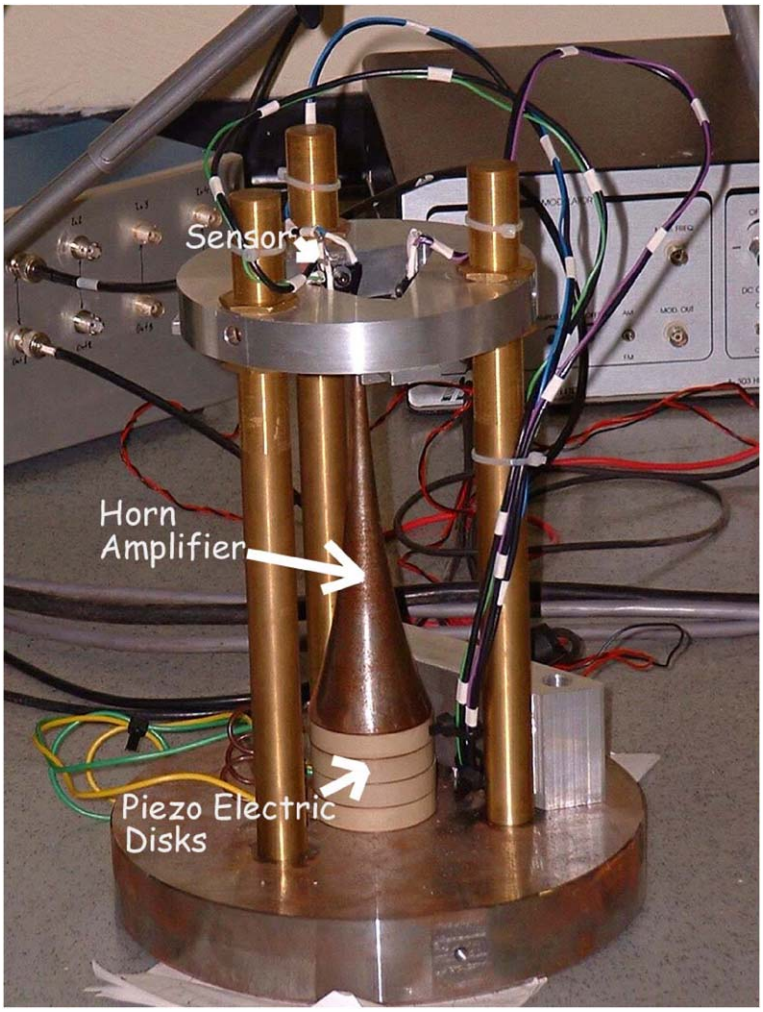

Fig. 13. The experimental system.

Initially the concavity constraint is not enforced and the effect of the change in the voltage amplitude is depicted in Fig. 15.

A change in the estimated frequency has been observed, but the convergence into a new amplitude level took around 150 iterations. The excitation frequency was increased, in this case, by the algorithm from 21 to 21.15 kHz.

Implementing the concavity constraint within the algorithm emphasises the importance of this constraint. Indeed, Fig. 16 demonstrates that the algorithm has become much faster and only after a few iterations a new optimal frequency estimate was established. The levitation height that was momentarily decreased has been regained after about 20 iterations.

To summarise the experimental study can state that the proposed algorithm seemed to fulfill its goal. Indeed, tracking of a suitable excitation frequency was achieved under realistic conditions.

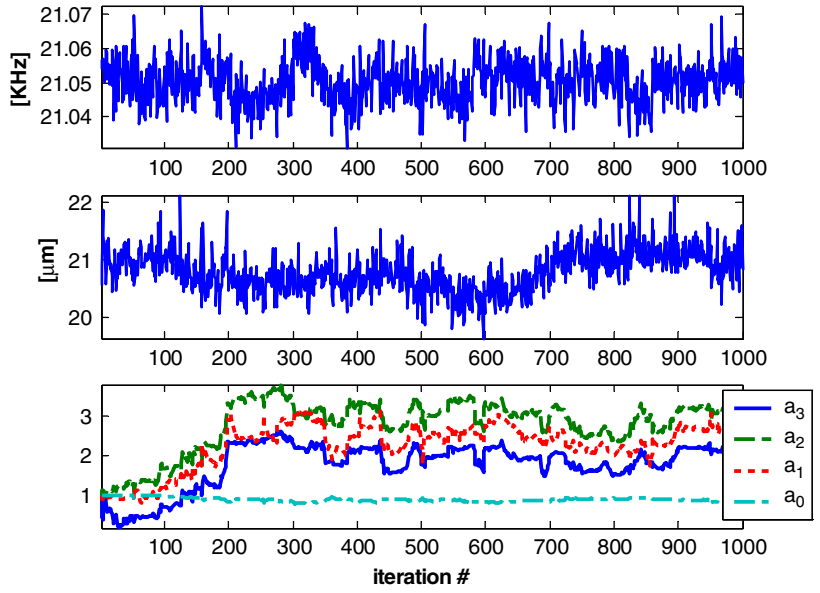

Fig. 14. Going through initialisation into steady-state mode in the experiment. No external parameter change. (Top): Injected frequency fluctuations. (Middle): The levitation gap. (Bottom): The polynomial coefficients.

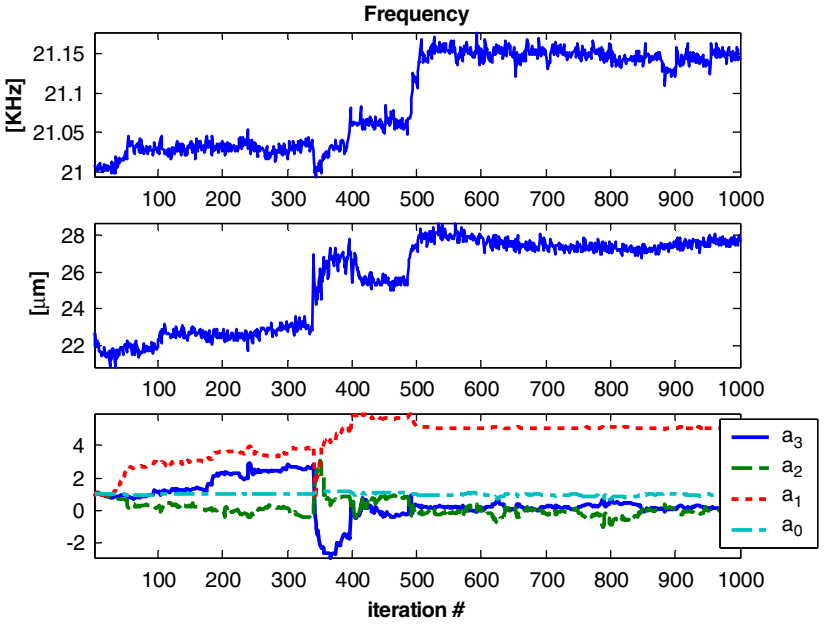

Fig. 15. Algorithm's behaviour when excitation amplitude is changed—no concavity constraint. (Top): The injected excitation frequency. (Middle): Levitation gap. (Bottom): The polynomial coefficients.

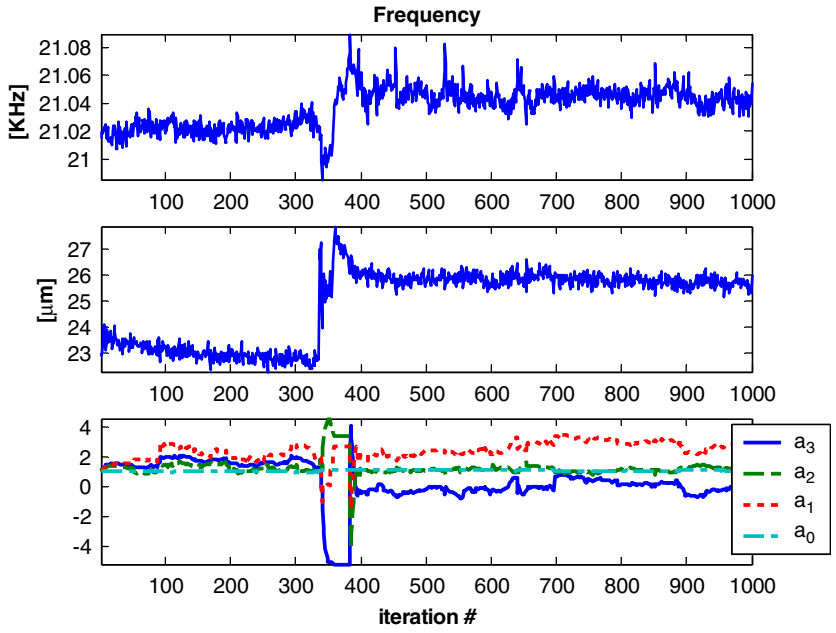

Fig. 16. Algorithm's behaviour when excitation amplitude is changed—with concavity constraint. (Top): The injected excitation frequency. (Middle): Levitation gap. (Bottom): The polynomial coefficients.

5. Conclusion

A resonance tracking algorithm combining a parametric identification with a numerical search for the optimal frequency of excitation was presented. The algorithm does not rely on linear systems' theory as it treats the measured response directly while curve-fitting in real-time a smoothed reduced model. The importance in understanding the numerical and physical behaviour was discussed and a feasible operating range was enforced to maintain levitation of the squeeze-film system. It was shown that adding dither to the algorithm actually improves its performance and a suitable analysis was presented showing how the dither can be chosen to achieve specified statistical performance.

This kind of algorithm can make a squeeze film levitation system smarter and still having more reliable performance. The proposed algorithm can also serve as a sensing mechanism detecting changes in the natural frequency for diagnostic purposes or as a method to minimise energy consumption while having as large as possible response levels.

Acknowledgements

The support of the fund for the promotion of research at the Technion (Grant No. 033-153) is gratefully acknowledged. The help of Dr. Adi Minikes in devising the numerical simulation and in the design of the experimental apparatus is thankfully acknowledged.

Appendix A

In this appendix, a proof for Eq. (8) is provided, showing that the (locally) optimal (in terms of efficiency) excitation frequency is one of the natural frequencies.

Expanding the amplitude of the response in Eq. (5) in terms of the normal modes:

$$U = \sum_{p=1}^{N} \alpha_p \psi_p, \tag{A.1}$$

where assume that

$$(-\omega_p^2 M_{uu} + H_{uu})\psi_p = 0, \quad p = 1 \ldots n \tag{A.2}$$

can obtain an expression for the real coefficients representing the contribution of the lth mode, by substituting Eq. (A.1) in Eq. (6):

$$\alpha_l = \left| \frac{\psi_l^T G e^{i(\theta-\beta)}}{\omega_l^2 - \omega^2 + i2\omega\zeta_l\omega_l} \right| = \frac{\psi_l^T G}{\sqrt{(\omega_l^2 - \omega^2)^2 + 4\zeta_l^2\omega^2\omega_l^2}}. \tag{A.3}$$

Using the definition of mechanical power in Eq. (7) and combining Eqs. (5), (6) with Eq. (A.2), the power, P, becomes

$$P = -i\omega U^T e^{i(\omega t-\theta)}(-\omega^2 M_{uu} + i\omega C_{uu} + H_{uu})U e^{i(\omega t-\theta)} \tag{A.4}$$

or

$$P = -i\omega U^T(-\omega^2 M_{uu} + i\omega C_{uu} + H_{uu})U. \tag{A.5}$$

When operating in the vicinity of a natural frequency, the amplitude is dominated by the corresponding eigenvector, hence choose $U = \alpha_l\psi_l$ ignoring the contribution of other modes.

Exploiting the well-known bi-orthonormality relations of eigenvectors [16, pp. 28–29], P can be expressed as

$$\begin{aligned} P &= i\omega\alpha_l\alpha_l(\omega_l^2 - \omega^2 + i\omega\psi_p^T C_{uu}\psi_q) \\ &= -i\omega\alpha_l\alpha_l(\omega_l^2 - \omega^2) + \alpha_l\alpha_l\omega^2\psi_l^T C_{uu}\psi_l \end{aligned} \tag{A.6}$$

or simplifying

$$P = -i\omega\alpha_l\alpha_l(\omega_l^2 - \omega^2) + 2\alpha_l\alpha_l\omega^2\zeta_l\omega_l. \tag{A.7}$$

The complex power can be separated into active and reactive terms

$$P_I = \omega\alpha_l\alpha_l(\omega_l^2 - \omega^2), \quad P_R = 2\alpha_l\alpha_l\omega^2\zeta_l\omega_l. \tag{A.8}$$

Defining the deviation of the excitation frequency from the natural frequency as $\Delta\omega = \omega_l - \omega$, one can obtain

$$\frac{P_R}{P_I} = \frac{2\zeta_l\omega\omega_l}{(\omega_l^2 - \omega^2)} = \frac{2\zeta_l\omega\omega_l}{(\omega_l - \omega)(\omega_l + \omega)} \approx \frac{\zeta_l\omega}{\Delta\omega}. \tag{A.9}$$

Indeed substituting Eq. (A.3) in Eq. (A.8) results

$$P_R = \psi_l^T G \frac{\psi_l^T G}{2\zeta_l \omega_l}, \quad P_I = \frac{\psi_l^T G}{2\zeta_l^2 \omega_l^2} \psi_l^T G \Delta\omega \tag{A.10}$$

and the total power $P = \sqrt{P_R^2 + P_I^2}$ in the vicinity of the natural frequency becomes

$$P = \frac{(\psi_l^T G)^2}{2\zeta_l \omega_l} \sqrt{1 + \left(\frac{\Delta\omega}{\zeta_l \omega_l}\right)^2}. \tag{A.11}$$

References

[1] J.S. Bendat, Nonlinear System Analysis and Identification From Random Data, Wiley-Interscience, New York, 1990.

[2] A. Minikes, I. Bucher, Coupled dynamics of a squeeze-film levitated mass and a vibrating piezoelectric disc: numerical analysis and experimental study, Journal of Sound and Vibration 263 (2003) 241–268.

[3] X. Sun, R. Horowitz, K. Komvopoulos, Stability and resolution analysis of a phase-locked loop natural frequency tracking system for MEMS fatigue testing, Journal of Dynamic Systems, Measurement and Control 124 (2002) 599–605.

[4] J. Tapson, J.R. Greene, Improved capacitance measurement by means of resonance locking, Measurement Science Technology 5 (1994) 20–26.

[5] J. Tapson, High precision, short range ultrasonic sensing by means of resonance mode-locking, Ultrasonics 33 (6) (1995) 441–444.

[6] P.E. Wellstead, M.B. Zarrop, Self-tuning Systems: Control and Signal Processing, Wiley, Chichester, 1991.

[7] R.A. Wannamaker, S.P. Lipshitz, J. Vanderkooy, J.N. Wright, A theory of nonsubtractive dither, IEEE Transactions on Signal Processing 48 (2) (2000).

[8] P. Zarchan, H. Gratt, Adaptive radome compensation using dither, Journal of Guidance, Control, and Dynamics 22 (1) (1999).

[9] D.V. Stallard, A missile adaptive roll autopilot with a new dither principle, IEEE Transactions on Automatic Control 11 (3) (1966) 368–378.

[10] E.O.J. Salbu, Compressible squeeze films and squeeze bearings, ASME Journal of Basic Engineering (1964) 355–366.

[11] R.E Best, Phase-Locked Loops, Design, Simulation, and Applications, fourth ed., McGraw-Hill, New York, UK, 1999.

[12] F.M. Gardner, Phase Lock Techniques, second ed., Wiley, New York, 1979.

[13] J.M. Mendel, Lessons in Estimation Theory for Signal Processing, Communication and Control, Prentice-Hall, PTR, Englewood Cliffs, NJ, 1995.

[14] L. Ljung, T. Söderström, Theory and Practice of Recursive Identification, MIT Press, Cambridge, MA, 1983.

[15] M. Naillon, R.H. Coursant, F. Besnier, Analysis of piezoelectric structures by finite elements method, ACTA Electronica 25 (4) (1983) 341–362.

[16] M. Geradin, D. Rixen, Mechanical Vibrations, Theory and Application to Structural Dynamics, Wiley, Chichester, 1997.

[17] C.T. Kelley, Iterative Methods for Optimization, SIAM, Philadelphia, PA, 1999.

[18] B. Widrow, S.D. Stearns, Adaptive Signal Processing, Prentice-Hall, Englewood Cliffs, NJ, 1985.

[19] S. Haykin, Adaptive Filter Theory, Prentice-Hall, Englewood Cliffs, NJ, 1986.

[20] C.L. Lawson, R.J. Hanson, Solving Least Squares Problems, Prentice-Hall, Englewood Cliffs, NJ, 1974.

[21] A. Björck, Numerical Methods For Least Squares Problems, SIAM, Philadelphia, 1996.

[22] H.S. Song, K. Nam, P. Mutschler, Very fast phase angle estimation algorithm for a single phase system having sudden phase angle jumps, IEEE-IAS, 13.-18.10.
[23] P.E. Gill, W. Murray, M.H. Wright, Practical Optimization, London Academic Press, London, 1981.
[24] R. Gabay, Resonance tracking method—application to a squeeze-film object levitation device, Master's Thesis, Technion - Israel Institute of Technology, May 2003 (in Hebrew).